An integrated valved microfluidic platform for rapid and simultaneous nucleic acid detection

Zihan Wang,‡ Fuwan Yang,‡ Shuai Zeng,‡ Rui Sun, Qifei Hu, Yichen Du*

Tianjin Key Laboratory of Life and Health Detection, Life and Health Intelligent Research Institute, Tianjin University of Technology, Tianjin, People's Republic of China

* Corresponding author

Email addresses: duyichen@email.tjut.edu.cn (Y. Du)

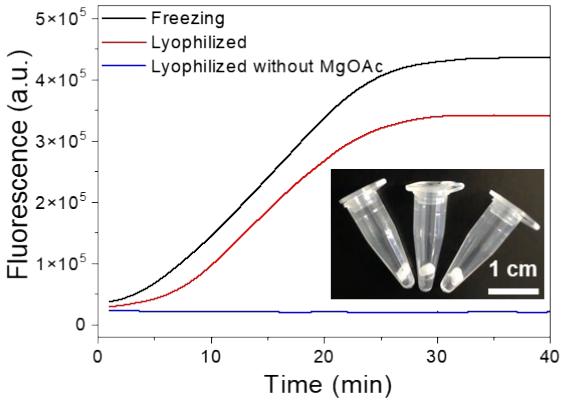

Fig. S1. Performance of RPA lyophilized reagent and morphology image of the lyophilized RPA reagent. The lyophilized RPA reagent was redissolved and mixed with Sybr Green I. Then the reaction is carried out at 37 °C in a real-time fluorescent PCR instrument (QuantStudio 3, Thermo Fisher), with fluorescence signals collected at 1-minute intervals.

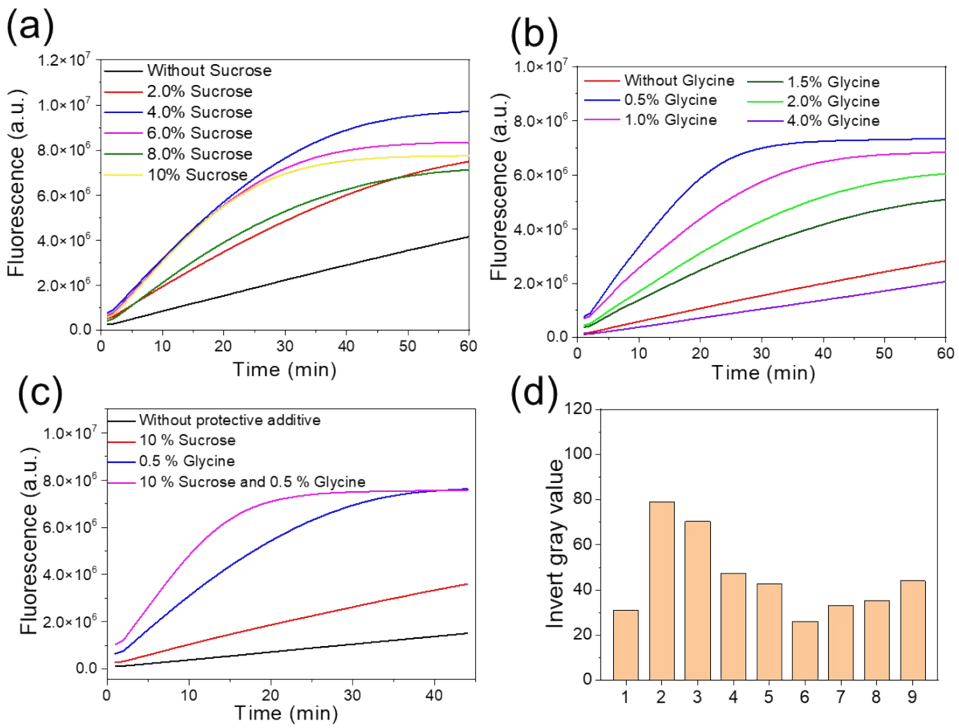

Fig. S2. Screening of different lyoprotectants for Cas12a. (a) Sucrose; (b) Protective effect of glycine; (c) Combination of lyoprotectants. Mixture containing 0.3 μL of LbCas12a (2 μM), 2 μL of F-Q (5 μM), 2 μL of crRNA (1 μM), 2 μL of NEBuffer 2.1 reaction buffer (10×), different lyoprotectants was frozen at -80°C for 20 minutes and lyophilized for 5 hours. The lyophilized Cas12a reagent was reconstituted with 18 μL of ultrapure water, followed by the addition of 2 μL of complementary sequence of the crRNA (C-crRNA). Then the reaction was carried out at 37 °C in a real-time fluorescent PCR instrument, with fluorescence signals collected at 1-minute intervals. (d) The grayscale values of the T lines from inverted scanned strip images of Fig. 1b.

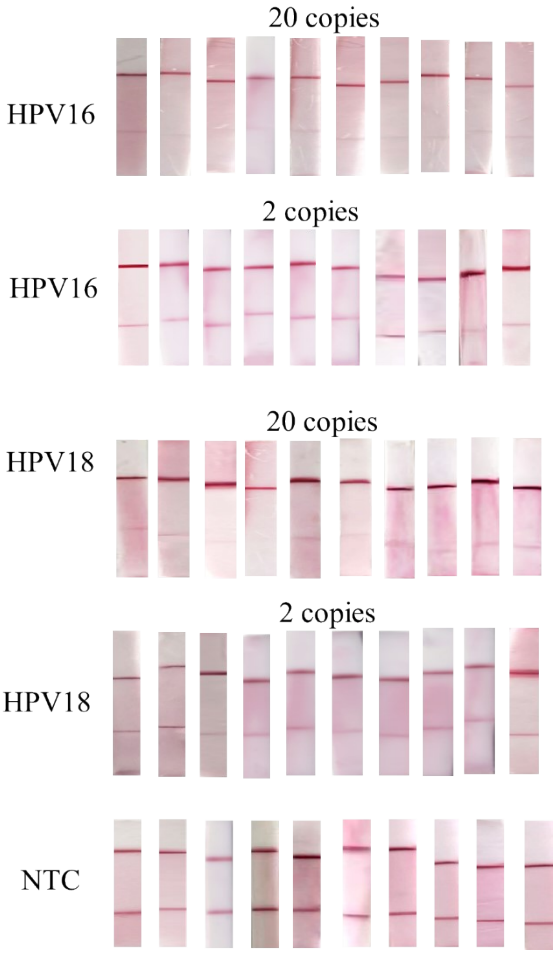

Fig. S3. Test strips of 10 independent replicates at target concentration of 20 copies, 2 copies and NTC (no-template control).

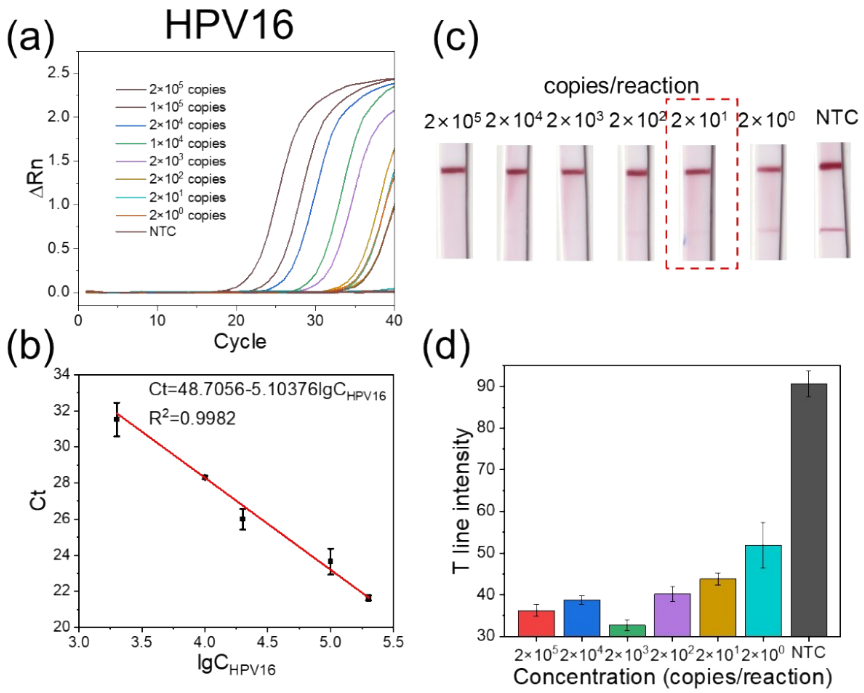

Fig. S4. (a) Detection of HPV16 plasmid by real-time quantitative PCR with primers HPV16L1-F and HPV16L1-R, employing the SYBR Green dye-based detection method. For clarity in visualization, amplification curves for higher target concentrations (2×10^3 to 2×10^5 copies/reaction) are shown from one representative replicate, while all three replicates are displayed for lower concentrations (2×10^2 to 0 copies/reaction) and the no-template control (NTC). (b) Linear fitting between Ct values and the logarithm of HPV16 plasmid concentration. (c) Detection results of HPV16 using non-lyophilized RPA-Cas12a lateral flow strips. (d) Grayscale values of the test line after inversion of the scanned strip images. Error bars represent standard deviation (n = 3).

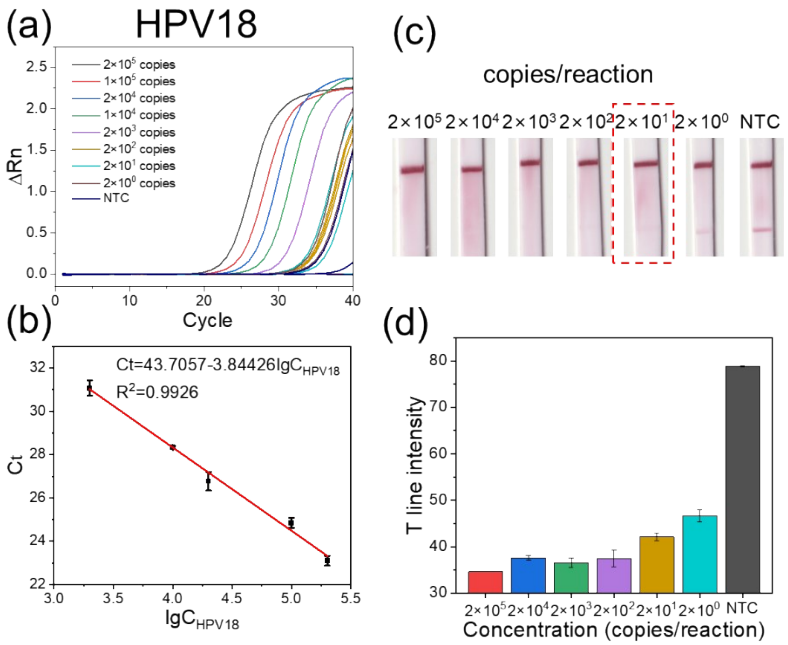

Fig. S5. (a) Detection of HPV18 plasmid by real-time quantitative PCR with primers HPV18-F and HPV18-R, employing the SYBR Green dye-based detection method. For clarity in visualization, amplification curves for higher target concentrations (2×10^3 to 2×10^5 copies/reaction) are shown from one representative replicate, while all three replicates are displayed for lower concentrations (2×10^2 to 0 copies/reaction) and the no-template control (NTC). (b) Linear fitting between Ct values and the logarithm of HPV18 plasmid concentration. (c) Detection results of HPV18 using non-lyophilized RPA-Cas12a lateral flow strips. (d) Grayscale values of the test line after inversion of the scanned strip images. Error bars represent standard deviation (n = 3).

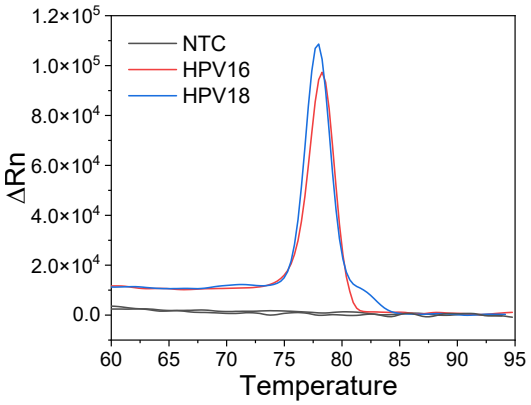

Fig. S6 qPCR melting curves. The melting curves were generated from real-time PCR assays conducted on QuantStudio 3 system (Thermo Fisher). Each 20 µL reaction contained 10 µL of Power SYBR™ Green PCR Master Mix, 1 µL of each forward and reverse primer (10 µM), and the HPV16 or HPV18 plasmid at a concentration of 2 × 10^5 copies per reaction. PCR amplification was performed with the following cycling protocol: 40 cycles of 94 °C for 15 s and 60 °C for 1 min. The distinct, single peaks observed for each target confirm the specificity of the primer sets and the absence of primer-dimers or non-specific amplification.

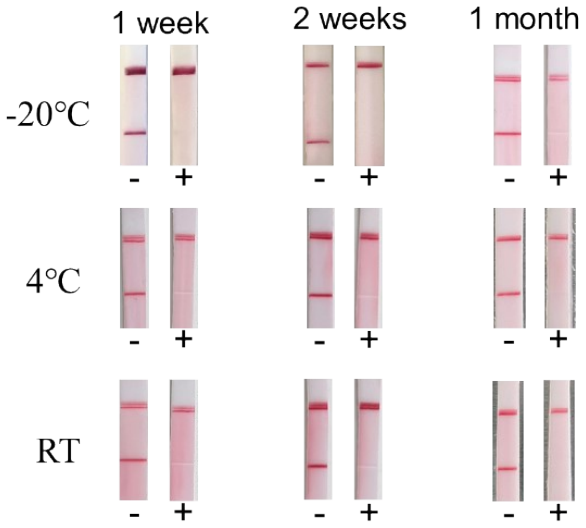

Fig. S7. Stability of RPA-CRISPR/Cas12a lyophilized reagents under different storage conditions.

(a)

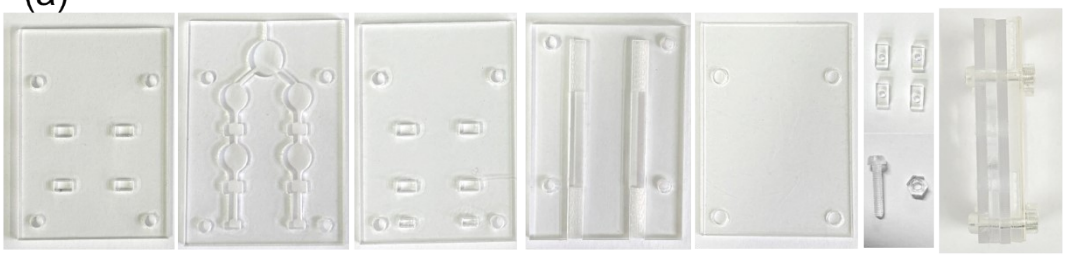

(b)

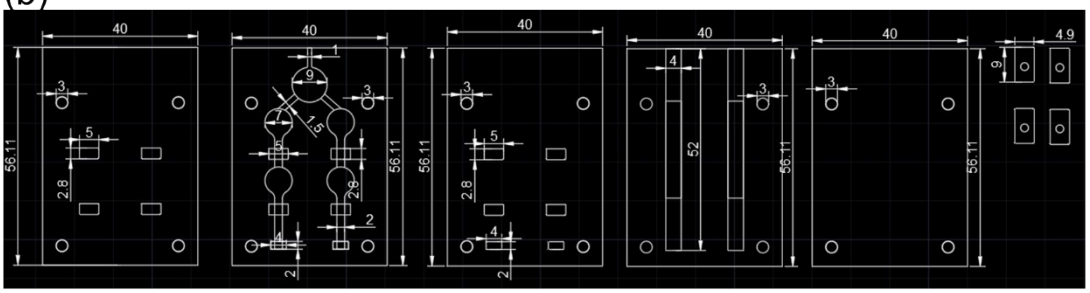

(c)

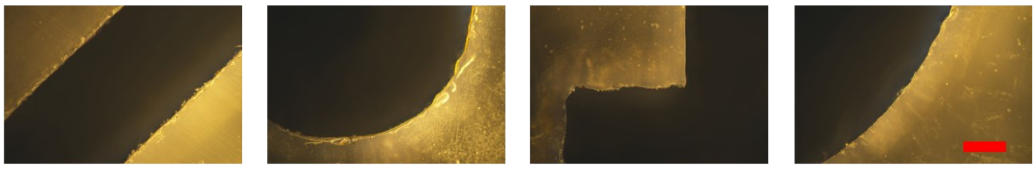

(d)

Measurement	Designed (mm)	Measured (mean±SD, mm)
Sample lysis chamber (Diameter)	9.00	8.90 ± 0.10
RPA chamber (Diameter)	7.00	6.92 ± 0.08
Liquid distribution channel (Width)	1.50	1.51 ± 0.03
Connecting channels (Width)	2.00	2.02 ± 0.02

Fig. S8. Schematic diagram of (a) each layer and (b) CAD. (c) Characterization of microfluidic chip features via metallographic microscopy. High-resolution images of the channels and reaction chambers. The scale bar was 500 μm. (d) Dimensional measurements on critical features across five independently fabricated chips.

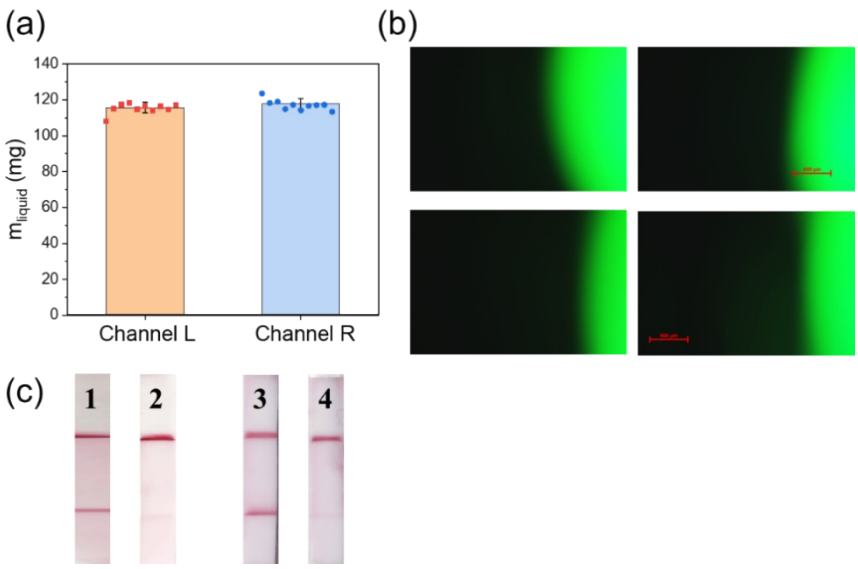

Fig. S9. (a) Experimental validation of uniform liquid distribution. Quantitative analysis of liquid mass distributed into the two chambers across ten independent replicates (n=10). The measurement was performed using a simplified, two-layer assembly of the device. Specifically, only the fluidic layer and the separation layer were assembled (without the detection layer). After the liquid flow process was complete, the liquid that had collected in the connecting channels at the bottom of the separation layer was carefully and fully recovered using a pipette. (b) Fluorescence images of the Fluorescein solution (0.8 mM) in the reaction chambers (up pictures) and channels (down pictures) were captured using a fluorescence microscope. The sharp fluorescence boundaries demonstrate the absence of liquid diffusion, confirming that the chambers are physically isolated during operation. The scale bar was 500 μm. (c) Positive controls and cross-contamination tests. 1: HPV16 RPA with 18-crRNA/Cas12a; 2: HPV16 RPA with 16-crRNA/Cas12a; 3: HPV18 RPA with 16-crRNA/Cas12a; 4: HPV16 RPA with 16-crRNA/Cas12a. The absence of positive signal in 1 and 3 (mismatched crRNA) confirms assay specificity and demonstrates the absence of cross-contamination between the parallel reaction chambers.

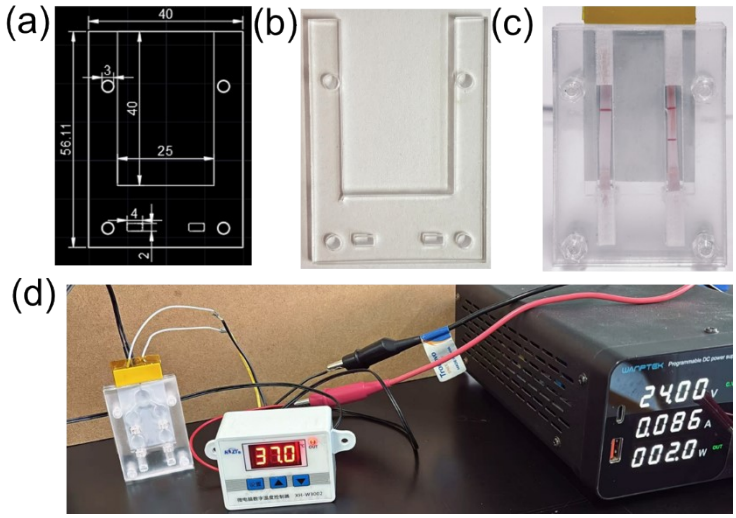

Fig. S10. Integration and performance validation of the on-chip heating system. (a) CAD design and the (b) photograph of the slot for inserting the thin-film heating pad. (c) Validation results obtained using the integrated heating system. (d) The assembled device is presented, showing the heating pad (supplier: Electric Heating Sensor Factory Store, Taobao) in place. The heating pad connected to a digital temperature controller (Model: XH-W3002, HAZY) and a power adapter (Model: TPS3010, WANPTEK).

Table S1 The oligonucleotides used in this work

Name	Sequence (5′→3′)
HPV16L1-F	GGT TAC AAC GAG CAC AGG GCC ACA ATA ATG GCA
HPV16L1-R	CCC ATG TCG TAG GTA CTC CTT AAA GTT AGT ATT TT
HPV16-crRNA	UAA UUU CUA CUA AGU GUA GAU UUA CUG UUG UUG AUA CUA CA
HPV18-F	GCA GGT GGT GGC AAT AAG CAG GAT ATT C
HPV18-R	CAA TTT CCA CTC CAG CAC AGG CCC ACA CTA
HPV18-crRNA	UAA UUU CUA CUA AGU GUA GAU UAA UCC UGA AAC ACA ACG
F-Q	FAM-CCCCCC-BHQ1
F-B	FAM-TTATTATT-Biotin
C-crRNA	TGTAGTATCAACAACAGCAA
HPV16L1 plasmid	GGTTACAACGAGCACAGGGCCACAATAATGGCATTTGTT GGGGTAACCAACTATTTGTTACTGTTGTTGATACTACACG CAGTACAAATATGTCATTATGTGCTGCCATATCTACTTCA GAAACTACATATAAAAATACTAACTTTAAGGAGTACCTA CGACATGGG
HPV18L1 plasmid	GCAGGTGGTGGCAATAAGCAGGATATTCCTAAGGTTTCT GCATACCAATATAGAGTATTTAGGGTGCAGTTACCTGAC CCAAATAAATTTGGTTTACCTGATACTAGTATTTATAATC CTGAAACACAACGTTTAGTGTGGGCCTGTGCTGGAGTGG AAATTG

The primers for HPV16 were adopted from a previously published and validated work.[1] The primers for HPV18 were designed in accordance with the manufacturer's (TwistDx) guidelines. To ensure high amplification efficiency, they were optimized by minimizing potential secondary structures using the mFold software.

References

[1] J. Gong, G. Zhang, W. Wang, L. Liang, Q. Li, M. Liu, L. Xue, G. Tang, A simple and rapid diagnostic method for 13 types of high-risk human papillomavirus (HR-HPV) detection using CRISPR-Cas12a technology. Sci Rep., 2021, 11, 12800. https://doi.org/10.1038/s41598-021-92329-2.